Measurements and Analysis of PLC Channels in a Cruise Ship

Massimo Antoniali, Andrea M. Tonello*, Matteo Lenardon, and Andrea Qualizza†
*DIEGM - Università di Udine - Via delle Scienze 208 - 33100 Udine - Italy
e-mail: massimo.antoniali@uniud.it, tonello@uniud.it
†FINCANTIERI - Cantieri Navali Italiani S.p.A. - Via Genova 1 - 34121 Trieste - Italy
e-mail: matteo.lenardon@fincantieri.it, andrea.qualizza@fincantieri.it

***Abstract*—Power line channel measurements and analysis in a cruise ship is the topic of this paper. Applications and benefits that the deployment of power line communication in a ship environment can bring, justify research initiatives targeting the study of channel characteristics. We have carried out a channel measurement campaign over the low voltage power distribution network of housing and public areas in the band 0-50 MHz. The data have been used to study the statistics of the channel, and in particular, of the average channel gain, RMS delay spread, coherence bandwidth. The analysis of theoretical capacity in the band 2-28 MHz (used by state-of-the art PLC technology) shows that it is in excess of 200 Mbps and up 600 Mbps depending on the background noise level and power line network segment of the ship. The capacity increases by up to 85% in the band 2-50 MHz. Furthermore, the three-phase electrical distribution allows the exploitation of multiple-input multiple-output transmission which can double the capacity as the results in this paper show.**

I. Introduction

Power line communications (PLC) have become increasingly popular in recent years. While outdoor and in-home PLC have raised significant interest for the possibility of delivering broadband Internet and high speed services without the need on new wires, in-vehicle PLC (which includes the in-car, in-plane and in-ship scenarios) is an application that has not been deeply investigated yet.

In this paper, we consider in-ship PLC which can provide significant benefits as the delivery of high speed communication services and the support of low speed command and control application without the need of dedicated cabling. Thus, it has the potential of simplifying the design of the communication network and more importantly saving weight and cost. In a typical cruise ship, 23% of the weight of the electrical system (3900 tonnes) is due to at least 30000 cables, for an overall length of 2400 km. Since the cruise ship is intrinsically a hotel and entertainment structure for passengers, multimedia services are of great interest. PLC can exploit the existing power distribution infrastructure to deliver high speed services to every cabin or to every deck [1].

For the proper design of a power line communication system, good knowledge of the channel characteristics is required. Only few papers deal with the characterization of in-ship PLC channels. In [2], the authors present a theoretical and experimental analysis on the application of PLC on a cruise ship developing a model based on a theoretical approach (in the band 0-12.5 MHz). In [3], the transfer function of a 440 V power line network in a container ship was measured and modeled in the frequency range 2-30 MHz. The characterization of the channels in training ships was reported in [4], while the study of unintentional radiations by PLC in ships and shipboard cables characteristics were the subjects of [5], [6]. Testing of HomePlug 1.0 compatible PLC modems in a cruise ship was conducting in [7].

In this paper, we summarize the results of a channel measurement campaign in a large cruise ship focusing on the LV distribution network in the band 0-50 MHz. The paper is organized as follows. Section II describes the cruise ship under test and the power distribution system. Section III explains the measurement setup and scenario. In Section IV, we deal with the statistical analysis of the channel, providing results in terms of insertion loss, average channel gain, RMS delay spread, coherence bandwidth and link capacity. The presence of three phase power distribution, allows the exploitation of multiple-input multiple-output transmission. Thus, the capacity of the 2x2 MIMO channel is also investigated. The effect of circuit breakers is briefly discussed in Section V. Finally, some conclusions follow.

II. Overview of the Ship Under Test and Power Distribution System

The measurement campaign has been done in a 116000 tonnes cruise ship built by Fincantieri. The electrical power generation and distribution system has been developed to satisfy the power needs of the electrical engines, lighting, in addition to all systems that have to guarantee correct functioning of hotel and entertainment structures. The power generation is ensured by asynchronous alternators moved by diesel engines. The generated medium voltage (MV) power (at 11 kV, 60 Hz) is first distributed to 9 MV/LV substations where it gets transformed in low voltage (LV) (690-440-220-115 V depending on the application). The LV electric power distribution system is a three-phase system with "insulated" and not distributed neutral.

As most of similar ships, our test ship is horizontally divided into two main areas: the engine areas located in lower decks, and housing and public areas that span 14 decks. Both areas

The work of M. Antoniali and A. M. Tonello has been partly supported by Rinave Consorzio per l'Alta Ricerca Navale within the project "Sistemi di Bordo con Tecnologia Power Line".

are also vertically divided. In particular, the housing and public areas are divided in fire zones by fire-resistant bulkheads. Each fire zone owns a MV/LV substation located on a deck beyond the decks of the engine zone. Power is distributed vertically from the switchboard of the substation to all decks of the same fire-zone reaching a number of distribution boards. Every distribution board is then connected by a bus-bar to a number of room service panels that serve a small number of rooms each.

III. Measurement setup and scenario

Channel measurements have been made in the time domain using a signal pulser and a digital oscilloscope with 50 Ω input impedance with sampling rate $F_s = 200$ Msamples/s. This realizes a single-input single-output (SISO) transmission since both the transmitter and the receiver are connected to test outlets between a pair of conductors. The capacitive coupler (for galvanic insulation) that we used has an almost flat frequency response up to about 50 MHz. The channel transfer function (ratio between the output and the input ports voltages up to 50 MHz), has been obtained via discrete Fourier transform (DFT) with a frequency step size of 100 kHz, i.e., processing channel responses of length 10 μs.

Giving the complexity and extension of the power line network in the test ship, we have divided the measurements in two sections as depicted in Fig. 1. The first section comprises the power line segment between a selected substation and a certain distribution board. The second section comprises the power line segment between the distribution board and a certain room service panel located in the same deck. We have selected one reference substation (among the 9 present in the test ship), that is located on deck n°4 and in fire-zone n°6. This substation is located in a barycentrical position and it is representative of the others in terms of wirings and topology of the housing and public areas. The switchboard of the selected

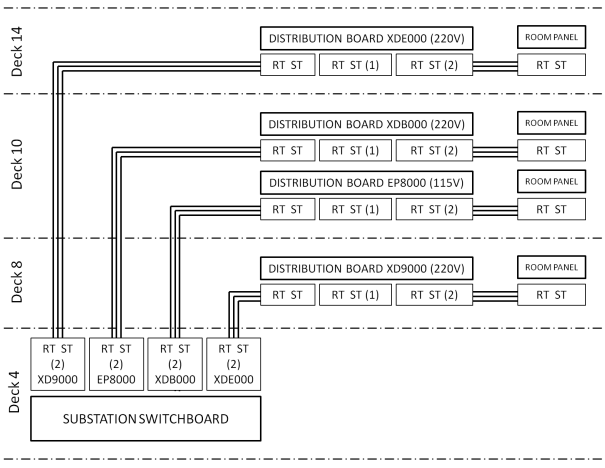

Fig. 1. Measurement scenario. RT and ST denotes test points with a coupler connected to R and T phases or between S and T phases. RT ST, RT ST (1) and RT ST (2) denote respectively test points at the input of the primary circuit breaker, at the output of it, and at the output of the secondary circuit breaker, respectively.

TABLE I
Measurement scenario cable properties

Distribution board	Deck	Length [m]	Section [mm^2]
XD9000 (220 V)	8	83	70
XDB000 (220 V)	10	79	70
EP8000 (115 V)	10	84	50
XDE000 (220 V)	14	95	70

substation supplies 45 distribution boards of the 220 V system, and 15 distribution boards of the 115 V system. Among all distribution boards, we have selected one located on deck n°8, two on deck n°10 (one for the 220 V system and one for the 115 V system) and another one on deck n°14. The armored power cables under test have variable section depending on the fact that they are used for the 220 V or the 115 V system. The cable properties are summarized in Table I. Finally, for each distribution board, we have selected one room service panel. The connection of the distribution board with the room service panel is realized by a bus-bar. Being the LV electric power distribution system a three-phase system with "insulated" and not distributed neutral, the direct and return channel have been realized by signaling on two phase wires. Since there are three available conductors (denoted with R, S, and T), two physical channels can be established. Thus, it is in principle possible to implement a 2x2 MIMO transmission. Consequently, we have measured both the direct channel and the coupled channel placing couplers both between the R and T conductors (RT) and between the S and T conductors (ST).

The substation switchboard, distribution boards and room service panels have a primary panel circuit breaker and a number of secondary circuit breakers equal to respectively the number of distribution boards, room service panels, and rooms connected to them. In the substation switchboard we have placed test points after the secondary circuit breakers (labeled with RT ST (2) in Fig. 1). In the distribution boards, we have placed test points at the input of the the primary circuit breaker, at the output of it, and at the output of the secondary circuit breaker (labeled with RT ST, RT ST (1) and RT ST (2) in Fig. 1). In the room panel we have placed the test point at the input of the primary circuit breaker.

IV. Statistical analysis

To ease the notation and for clarity, we denote with SS-DB the connection of the substation switchboard with the distribution boards, while with DB-RP the connection between the distribution boards and the room service panels. The statistical analysis of data is done in the band 0-50 MHz, unless differently specified.

A. Insertion Loss

We provide results firstly in terms of insertion loss (IL) that is defined as $IL = |H(f)|^2$ and its version in dB as $IL_{|dB} = 10\log_{10}(|H(f)|^2)$ where $H(f) = H_{(TX,RX)}(f)$ is the channel transfer function (CTF) between the transmitter

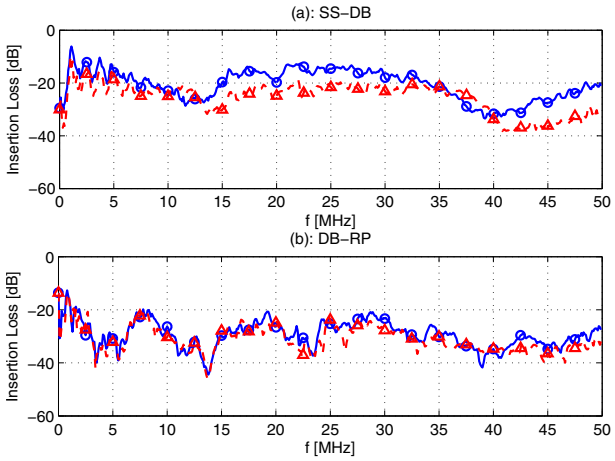

Fig. 2. 50-th percentile of insertion loss of SS-DB links in subplot (a), and DB-RP in subplot (b). Solid curves refer to direct links, dashed curves to coupled ones.

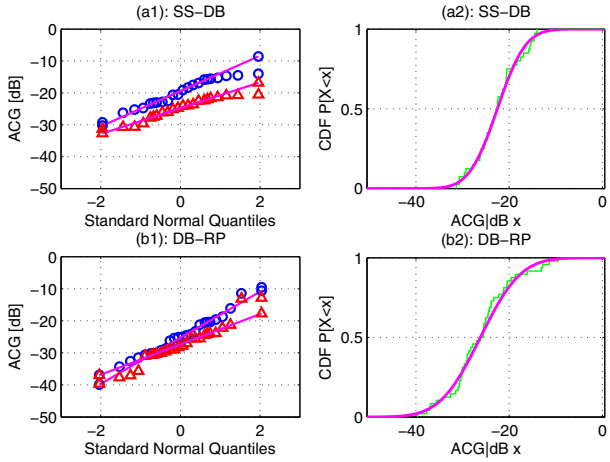

Fig. 3. (a1), (b1): Quantile-quantile plots of $ACG_{|dB}$ of the SS-DB and DB-RP channels. Direct links with blue circled markers, coupled links with triangular red markers. (a2), (b2): CDF of $ACG_{|dB}$ of the SS-DB and DB-RP channels.

TABLE II
STATISTICAL VALUES OF MEASURED AVERAGE CHANNEL GAIN IN dB

$ACG_{\|dB}$	Min	Max	Mean	Std deviation
SS-DB direct	-29.29	-13.99	-20.0116	4.50
SS-DB coupled	-31.31	-20.57	-25.06	3.54
SS-DB	-31.31	-13.95	**-22.54**	**4.74**
DB-RP direct	-36.88	-9.47	-24.80	6.84
DB-RP coupled	-39.65	-12.84	-27.54	6.56
DB-RP	-39.65	-9.48	**-26.17**	**6.78**

TX and the receiver RX with $TX, RX \in \{RT, ST\}$ depending on the phases involved in the link.

In Fig. 2, we show the 50-th percentile (median value) of the IL in dB scale over all measured links as function of frequency. In subplot (a), we report results for the SS-DB links, while in subplot (b), for the DB-RP links. The direct channels, i.e., (RT, RT) or (ST, ST), are with solid lines, while the coupled channels, i.e., (RT, ST) or (ST, RT), are with dashed lines. The figure shows that the frequency dependence and attenuation is more significant for DB-RP links due to larger presence of branches and discontinuities and related impedance mismatches. Furthermore, the IL of the direct and coupled channels for the DB-RP links are similar. We speculate that this behavior is due to the bus-bar system topology.

B. Average Channel Gain

The average channel gain (ACG) is computed by averaging the IL as follows

$$ACG = \frac{1}{N}\sum_{n=0}^{N-1}\left|H\left(\frac{n}{NT_s}\right)\right|^2 = \sum_{n=0}^{N-1}|h(nT_s)|^2 \quad (1)$$

where $H(n/NT_s)$ is the CTF obtained as the N-points DFT of the impulse response $h(nT_s)$ sampled at rate $F_s = 1/T_s = 200$ MHz, $T_s = 5$ ns is the sampling time resolution, and $N = 2000$ is the number of impulse response points. The ACG in dB scale is defined as $ACG_{|dB} = 10\log_{10}(ACG)$. In Table II, we report the minimum value, the maximum value, the mean, and the standard deviation of the $ACG_{|dB}$ for the SS-DB links and for the DB-RP links (direct, coupled, and all together). In Fig. 3, we report the quantile-quantile plots of the $ACG_{|dB}$ for the SS-DB link (subplot (a1)) and for the DB-RP link (subplot (b1)), to test the normality of the distribution function of the $ACG_{|dB}$. These curves report the measured samples against a similar number of quantiles taken from a normal distribution. If the samples are drawn from a normal distribution, the curve will be linear. The figure proves that the ACG in dB is normal.

In the subplots (a2) and (b2) of Fig. 3, we show the cumulative distribution function (CDF) of the $ACG_{|dB}$ for the SS-DB and DB-RP links (direct and coupled ones all together) compared to CDFs of two random variables normally distributed with mean and standard deviation reported in Table II (bold values).

It follows, that the ACG (in linear scale) is lognormally distributed with good approximation. The same distribution has been found in the analysis of PLC channels of the in-home scenario [8], [9], [10].

C. RMS Delay Spread

The RMS delay spread RMS-DS is the square root of the second central moment of the power-delay profile, defined as follows

$$\sigma_\tau = \sqrt{\mu_\tau'' - \mu_\tau^2} \quad (2)$$

with

$$\mu_\tau = \frac{\sum_{n=0}^{N-1} nT_s\,|h(nT_s)|^2}{\sum_{n=0}^{N-1}|h(nT_s)|^2} \qquad \mu_\tau'' = \frac{\sum_{n=0}^{N-1}(nT_s)^2\,|h(nT_s)|^2}{\sum_{n=0}^{N-1}|h(nT_s)|^2}. \quad (3)$$

It is used to measure the multipath spread and characterize the effect of channel dispersion on a transceiver. In the following, we denote the RMS-DS in μs as $\sigma_{\tau|\mu s}$. In Table III, we report

TABLE III
STATISTICAL VALUES OF MEASURED RMS DELAY SPREAD IN μs

$\sigma_{\tau\|\mu s}$	Min	Max	Mean	Std deviation
SS-DB direct	0.22	0.97	0.54	0.21
SS-DB coupled	0.33	1.05	0.68	0.22
SS-DB	0.22	1.05	**0.61**	**0.22**
DB-RP direct	0.24	1.20	0.69	0.25
DB-RP coupled	0.43	1.55	0.83	0.33
DB-RP	0.24	1.55	**0.76**	**0.30**

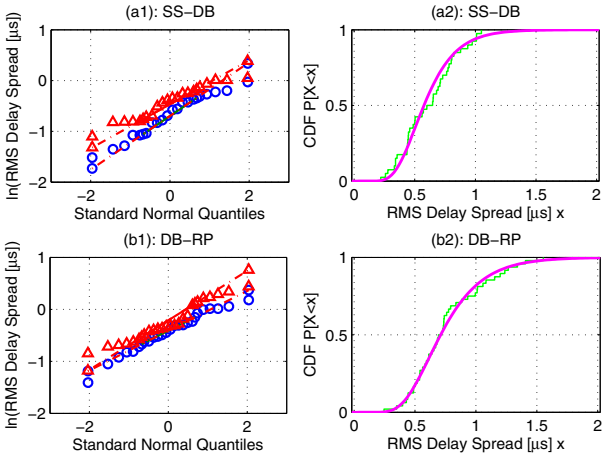

Fig. 4. (a1), (b1): Quantile-quantile plots of $\ln(\sigma_{\tau|\mu s})$ of the SS-DB and DB-RP channels. Direct channels are marked with blue circles, while coupled channels with red triangles. (a2), (b2): CDFs of $\sigma_{\tau|\mu s}$ of SS-DB and DB-RP channels.

the minimum value, the maximum value, the mean, and the standard deviation of $\sigma_{\tau|\mu s}$. The RMS-DS can be considered lognormal distributed with good approximation as the linear trend in the quantile-quantile plots of its logarithmic version in Fig. 4 (a1) and (b1) show.

The CDFs of the RMS-DS of SS-DB and DB-RP channels are reported in Fig. 4.a2 and Fig. 4.b2 . They are compared to the CDFs of two lognormal distributed random variables with mean and standard deviation reported in Table III (bold values).

We now investigate the relationship between the RMS-DS and the ACG. The RMS-DS and the ACG are negatively correlated. Therefore, channels with large RMS delay spread are also characterized by small average channel gain (large attenuation) [8]. Fig. 5 shows a scatter plot of $\sigma_{\tau|\mu s}$ versus $ACG_{|dB}$, and the trend line evaluated by minimizing the mean square error between the trend line and the observed values. The relations of the trend line are

$$\sigma_{\tau|\mu s}^{(SS-DB)} = -0.0274\, ACG_{|dB}^{(SS-DB)} \quad (4)$$

$$\sigma_{\tau|\mu s}^{(DB-RP)} = -0.0287\, ACG_{|dB}^{(DB-RP)}. \quad (5)$$

Circled data points belong to the measurements of direct links, triangular ones belong to the coupled links. The scatter plot shows that SS-DB channels are characterized by $\sigma_{\tau|\mu s}$

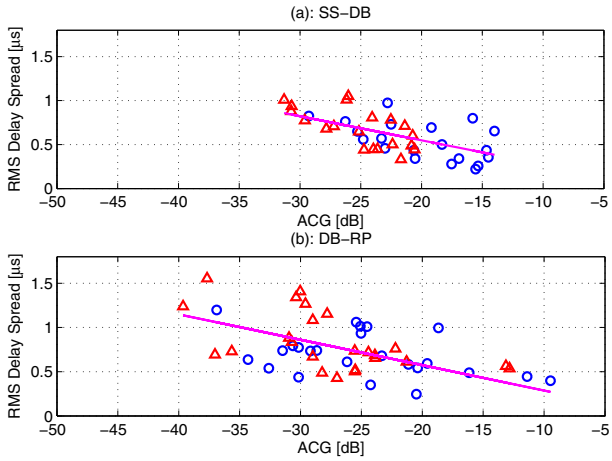

Fig. 5. Scatter plot of $\sigma_{\tau|\mu s}$ versus $ACG_{|dB}$ and evaluated trend line for the SS-DB and DB-RP channels. Direct realizations are marked with blue circles, while coupled channels with red triangular markers.

and $ACG_{|dB}$ values concentrated around the mean values, while for DB-RP channels the values are more spread. The correlation coefficient between $\sigma_{\tau|\mu s}^{(SS-DB)}$ and $ACG_{|dB}^{(SS-DB)}$ is -0.64, while between $\sigma_{\tau|\mu s}^{(DB-RP)}$ and $ACG_{|dB}^{(DB-RP)}$ is - 0.51 .

D. Coherence bandwidth

The frequency selective behavior of the channel can be analyzed in terms of the autocorrelation function (ACF) of the frequency response that is defined as

$$R(\Delta f) = \int_B H(f)H^*(f+\Delta f)df \quad (6)$$

where * denotes the complex conjugate, Δf is the frequency shift and B = [0 50] MHz is the channel band. The coherence bandwidth is a statistical measure of the range of frequencies over which two frequency components of the channel have a generally accepted value of correlation, e.g., equal to 0.9 and 0.7.

In Tables IV and V, we report the coherence bandwidth statistical values for all measured channels with a correlation index equal to 0.9 and 0.7. Quantities are in kHz scale. In Fig. 6, we show the scatter plots of the RMS-DS versus the coherence bandwidth $BC_{0.9|kHz}$ and $BC_{0.7|kHz}$, respectively

TABLE IV
STATISTICAL VALUES OF MEASURED COHERENCE BANDWIDTHS $BC_{0.9}$ IN kHz

$BC_{0.9\|kHz}$	Min	Max	Mean	Std deviation
SS-DB direct	70	1290	344.50	405
SS-DB coupled	60	320	152	77.64
SS-DB	60	1290	248.25	303.89
DB-RP direct	40	410	149.17	107.25
DB-RP coupled	20	240	111.67	64.25
DB-RP	20	410	130.42	89.49

TABLE V
STATISTICAL VALUES OF MEASURED COHERENCE BANDWIDTHS $BC_{0.7}$ IN kHz

$BC_{0.7\|kHz}$	Min	Max	Mean	Std deviation
SS-DB direct	230	4390	2012	1652.40
SS-DB coupled	190	3110	1374	1198.10
SS-DB	190	4390	1693	1460.8
DB-RP direct	130	2520	517.08	561.42
DB-RP coupled	80	940	377.08	244.37
DB-RP	80	2520	447.08	434.13

for SS-DB channels ((a1) and (a2) subplots), and DB-RP ones ((b1) and (b2) subplots). The relations between $\sigma_{\tau|\mu s}$ and $BC_{0.9|kHz}$ and $BC_{0.7|kHz}$ can be approximated as hyperbolic relations. By fitting the simulation results, we propose the following relations, obtained minimizing the mean square error between the trend lines and the observed values

$$\sigma_{\tau|\mu s}^{(SS-DB)} = \frac{74}{BC_{0.9|kHz}^{(SS-DB)}} \tag{7}$$

$$\sigma_{\tau|\mu s}^{(SS-DB)} = \frac{236}{BC_{0.7|kHz}^{(SS-DB)}} \tag{8}$$

$$\sigma_{\tau|\mu s}^{(DB-RP)} = \frac{51}{BC_{0.9|kHz}^{(DB-RP)}} \tag{9}$$

$$\sigma_{\tau|\mu s}^{(DB-RP)} = \frac{180}{BC_{0.7|kHz}^{(DB-RP)}}. \tag{10}$$

E. Capacity

In this section we evaluate the potential transmission performance in terms of link capacity C in the Home Plug AV frequency band [11] 2-28 MHz and in the band 2-50 MHz under the assumption of a transmitted signal power spectral density (PSD) $P_{TX} = -50$ dBm/Hz and white Gaussian background noise with PSD $P_N = -110$ dBm/Hz or with $P_N = -140$ dBm/Hz, i.e.,

$$C = \Delta f \sum_{i=1}^{N_c} \log_2 \left(1 + \frac{P_{TX}|H(f_i)|^2}{P_N}\right). \tag{11}$$

The sub-carriers are spaced by $\Delta f = 24.414$ kHz, with number $N_c = 1064$ in the HPAV frequency band while $N_c = 1961$ in the frequency band 2-50 MHz. $H(f_i)$ is the CTF evaluated at the $i-$subcarrier frequency. Measurements of the noise has shown that it ranges between the two considered values of PSD depending on the location and the devices operating on board of the ship.

In Fig. 7, we report the complementary cumulative distribution function (CCDF) of the channel capacities for the SS-DB links in subplots (a1) and (a2), for the DB-RP links in subplots (b1) and (b2), in considered frequency bands. It is possible to notice that the SS-DB links are those that statistically convey higher rate than DB-RP links. In the HPAV band, for the SS-DB links, the 70-th percentile of the CCDF curve is equal to 330 Mbps and 290 Mbps, respectively for the direct and the coupled channels with $P_N = -110$ dBm/Hz, and it is equal to 590 Mbps and 550 Mbps with $P_N = -140$ dBm/Hz. For DB-RP links, the 70-th percentile of the CCDF curve is equal to 240 Mbps and 220 Mbps, respectively for direct and coupled channels with $P_N = -110$ dBm/Hz, and it is equal to 490 Mbps and 470 Mbps with $P_N = -140$ dBm/Hz. Even if DB-RP links convey lower rate, we have noted that the capacity of coupled channels is still 90-96% of the capacity of direct ones. The relatively small loss in capacity of the coupled channels, is due to the bus-bar system topology. This yields an advantage in practical scenarios where the modem placed in the rooms can be connected to different pair of phases. In the 2-50 MHz band, performances increase by up to 70% for SS-DB links and by up to 85% for DB-RP ones.

Since three phases are available, 2x2 MIMO transmission is possible. It should be noticed that a 2x2 MIMO transmission

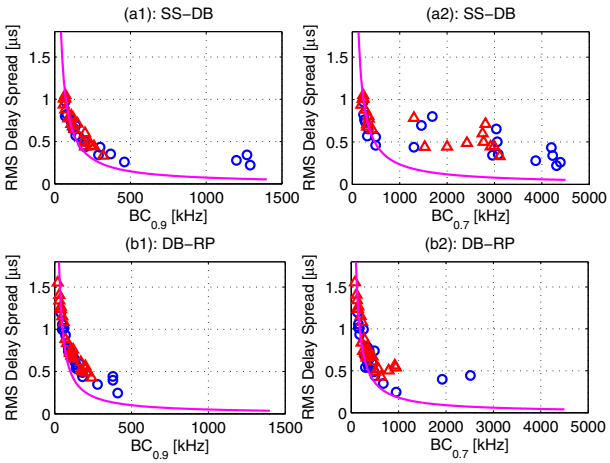

Fig. 6. RMS Delay Spread as a function of $BC_{0.9|kHz}$ and $BC_{0.7|kHz}$ for SS-DB links (a1)-(a2), and for DB-RP links (b1)-(b2).

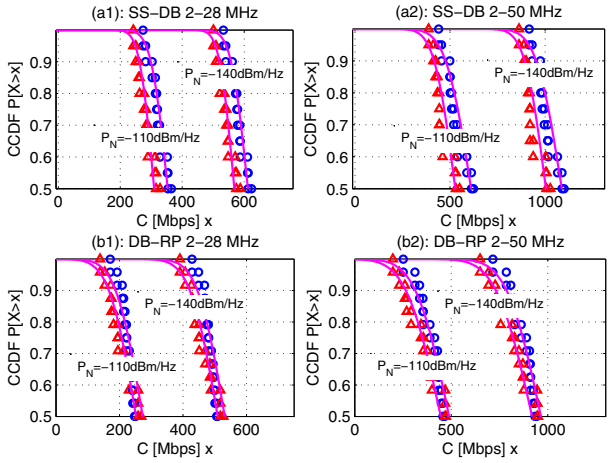

Fig. 7. CCDF of capacity for SS-DB links (a1)-(a2), and DB-RP links (b1)-(b2), for two different noise PSD levels and frequency bands. Direct channels marked with blue circles, coupled channels marked with red triangles.

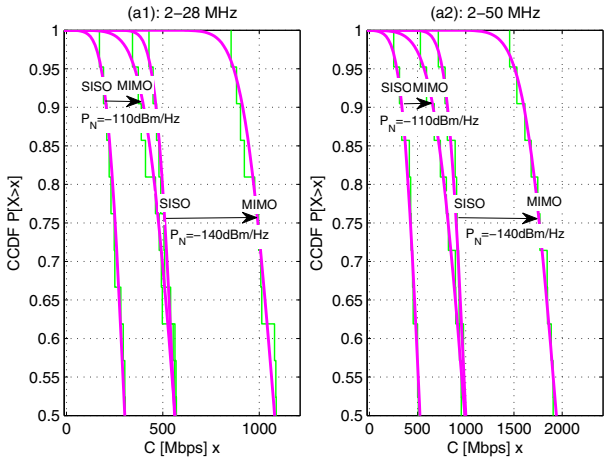

Fig. 8. CCDF of capacity for SISO and MIMO transmission for two different noise PSD levels and frequency band 2-28 MHz (a1) and 2-50 MHz (a2).

scheme implies that two signals are simultaneously transmitted in the two transmitting ports (between the RT conductors and ST conductors) and received in the two receiving ports. In our measurement campaign, the direct and coupled channels have been measured in a SISO transmission mode, i.e., leaving open the remaining input and output ports. Thus, the numerical results yield only an indication of the achievable capacity. To proceed, the overall channel transfer function (ratio between the output and the input ports voltages) matrix of the MIMO transmission scheme $\mathbf{H}(f)$ is defined as

$$\mathbf{H}(f) = \begin{bmatrix} H_{(RT,RT)}(f) & H_{(RT,ST)}(f) \\ H_{(ST,RT)}(f) & H_{(ST,ST)}(f) \end{bmatrix} \qquad (12)$$

where $H_{(TX,RX)}$ is a SISO channel CTF with $TX, RX \in \{RT, ST\}$ denoting transmitting port and receiving one. Under the same assumptions in (11), the MIMO capacity reads

$$C_{MIMO} = \Delta f \sum_{i=1}^{N_c} \log_2 \left[\det \left(\mathbf{U} + \frac{P_{TX}}{2P_N} \mathbf{H}_i \mathbf{H}_i^H \right) \right] \qquad (13)$$

where $\mathbf{U}$ is the 2x2 identity matrix, $\mathbf{H}_i$=$\mathbf{H}(f_i)$ and ^{H} denotes the hermitian transpose. In Fig. 8, we report the CCDF of the MIMO channel capacities achievable over all links (SS-DB and DB-RP) assuming a constant transmit PSD equal to $P_{TX} = -50$ dBm/Hz, and two different values for the noise PSD, i.e., $P_N = -110$ dBm/Hz and $P_N = -140$ dBm/Hz in the frequency band 2-28 MHz (a1) and 2-50 MHz (a2). On average, the MIMO channel yield a capacity that is double that of the SISO channel, in both considered frequency bands.

V. Effect of circuit breakers

Although not reported for space limitation, we have also studied the effect of the distribution board circuit breakers. On average, the attenuation due to primary and secondary circuit breakers is approximately 7 dB.

VI. Conclusion

We have reported the results of a measurement campaign on board of a cruise ship over the low voltage power grid. The analysis shows that the channel statistics are similar to those reported in other application scenarios, e.g., the in-home scenario. In particular, the average channel gain and the RMS delay spread are lognormally distributed. However, the mean values are somewhat higher than those found in the in-home case. Nevertheless, the LV in-ship channels can carry high amount of data information as the analysis of the capacity shows. This is in excess of 200 Mbps and up to about 600 Mbps for the band 2-28 MHz depending on the noise conditions and on the power grid section. It increases by up to 85% in the band 2-50 MHz. In particular, the links between the MV/LV substation and the distribution boards have higher capacity than the links between the distribution boards and the room service panels. This can be justified by the fact the latter scenario is characterized by a topology with more branches which causes higher frequency selectivity and fading. Theoretical capacity can be approximately doubled if a MIMO transmission scheme is used, which is applicable to three-phase electrical power distribution system.

References

[1] S. Tsuzuki, M. Yoshida, Y. Yamada, H. Kawasaki, K. Murai, K. Matsuyama, and M. Suzuki, "Characteristics of Power-Line Channels in Cargo Ships," in *Proc. IEEE Int. Symp. Power Line Commun. and its App.*, Mar. 2007, pp. 324-329.

[2] S. Barmada, L. Bellanti, M. Raugi, and M. Tucci, "Analysis of Power-Line Communication Channels in Ships," in *IEEE Trans. Vehicular Technology*, Vol. 59 , n. 7, Sept. 201, pp. 3161-3170.

[3] J. Nishioka, S. Tsuzuki, M. Yoshida, H. Kawasaki, T. Shinpo, and Y. Yamada, "Characteristics of 440V Power-Line Channels in Container Ships," in *Proc. IEEE Int. Symp. Power Line Commun. and its App.*, Mar.-Apr. 2009, pp. 217-222.

[4] M. Yoshida, S. Tsuzuki, Y. Yamada, K. Murai, M. Takechi, K. Matsuyama, T. Shinpo, Y. Saito, and S. Takaoka, "Characteristics of Power-Line Channels in the Training Ship YUGEMARU," IEICE Technical Report, Vol. 07, N. 257, WBS2007-46, Oct. 2007, pp. 41-46. (In Japanese)

[5] M. Yoshida, S. Tsuzuki, Y. Yamada, H. Kawasaki, K. Murai, K. Matsuyama, T. Shinpo, Y. Saito, and S. Takaoka, "A Study of Unintentional Radiation by PLC in Ships," in *Proc. Electronics, Information and Systems Society Conference*, Sept. 2007. (In Japanese)

[6] S. Tsuzuki, M. Yoshida, Y. Yamada, K. Murai, H. Kawasaki, K. Matsuyama, T. Shinpo, Y. Saito, and S. Takaoka, "Channel Characteristic Comparison of Armored Shipboard Cable and Unarmored one," in *Proc. IEEE Int. Symp. Power Line Commun. and its App.*, Apr. 2008, pp. 7-12.

[7] E. Liu, Y. Gao, G. Samdani, O. Mukhtar, and T. Korhonen, "Powerline Communication over Special Systems," in *Proc. IEEE Int. Symp. Power Line Commun. and its App.*, Apr. 2005, pp. 167-171.

[8] S. Galli, "A Simplified Model for the Indoor Power Line Channel," in *Proc. IEEE Int. Symp. Power Line Commun. and its App.*, Apr. 2009, pp. 13-19.

[9] A. M. Tonello, and F. Versolatto, "Bottom-Up Statistical PLC Channel Modeling-Part II: Inferring the Statistics," in *IEEE Trans. Power Del.*, Vol. 25, n. 4, October 2010, pp. 2356-2363.

[10] A. M. Tonello, "Brief Tutorial on the Statistical Top-Down PLC Channel Generator" [Online]. Available: http://www.diegm.uniud.it/tonello/PAPERS/WHITE/TUTORIAL_CHAN_2010.pdf

[11] HomePlug AV white paper [Online]. Available: http://www.homeplug.org.